Journal of Computational Neuroscience 4, 161–172 (1997)

The Role of Axonal Delay in the Synchronization of Networks of Coupled Cortical Oscillators

S.M. CROOK
Department of Mathematics, University of Maryland, College Park, MD 20742
Mathematical Research Branch, NIDDK, National Institutes of Health, Bethesda, MD 20814
crook@bart.niddk.nih.gov

G.B. ERMENTROUT
Department of Mathematics, University of Pittsburgh, Pittsburgh, PA 15260
bard@mthbard.math.pitt.edu

M.C. VANIER
Division of Biology, Computation and Neural Systems Program, California Institute of Technology, Pasadena, CA 91125
mvanier@bbb.caltech.edu

J.M. BOWER
Division of Biology, California Institute of Technology, Pasadena, CA 91125
jbower@bbb.caltech.edu

Received May 1, 1996; Revised October 9, 1996; Accepted October 15, 1996

Action Editor: Larry Abbott

Abstract. Coupled oscillator models use a single phase variable to approximate the voltage oscillation of each neuron during repetitive firing where the behavior of the model depends on the connectivity and the interaction function chosen to describe the coupling. We introduce a network model consisting of a continuum of these oscillators that includes the effects of spatially decaying coupling and axonal delay. We derive equations for determining the stability of solutions and analyze the network behavior for two different interaction functions. The first is a sine function, and the second is derived from a compartmental model of a pyramidal cell. In both cases, the system of coupled neural oscillators can undergo a bifurcation from synchronous oscillations to waves. The change in qualitative behavior is due to the axonal delay, which causes distant connections to encourage a phase shift between cells. We suggest that this mechanism could contribute to the behavior observed in several neurobiological systems.

Keywords: axonal delay, cortical oscillators, phase, synchrony, coupled oscillators

1. Introduction

For the last several years there has been growing interest in the mechanisms underlying the oscillatory properties of the mammalian cerebral cortex (Gray, 1994). It is now apparent that oscillations in all regions of the cortex have remarkably common temporal characteristics with dominant frequencies centered around

the 40 Hz (gamma) frequency range and the 7–10 Hz (theta) frequency range. These similarities in the frequency domain presumably reflect similarities in the neuronal components of the cerebral cortex. Several groups have proposed that these frequencies are under the direct influence of the time constants of inhibitory mechanisms within the cortical circuitry (Bower, 1995; Wilson and Bower, 1992; Whittington et al., 1995). Evidence suggests that there is more variability in the spatial domain. For example, it has been demonstrated that neocortical oscillations such as those in the visual cortex tend to be synchronous (Gray et al., 1989) while the piriform or olfactory cortex tends to exhibit traveling waves of oscillations (Haberly, 1985; Freeman, 1978). Based on their cortical models, Wilson and Bower (1991, 1992) previously proposed that these differences in the spatial organization of cortical oscillations may be partially due to the properties of axonal coupling. In particular, they found that strengthening the long-range coupling results in less synchronous oscillatory activity.

One of the goals of this article is to explain this seemingly contradictory result in which synchrony is stable for localized excitatory coupling but long-range coupling leads to an unstable synchronous state. We do this using a coupled neural oscillator model with a single phase variable representing the behavior of each individual oscillator. Many recent studies use this technique to develop qualitative models of system behavior; however, most such models involve the coupling of a few discrete units or chains of discrete units and are concerned with the development of synchrony and phase shifts in small populations where boundary effects play a major role in the evolution of the behavior. Kopell and Ermentrout (1986; Ermentrout and Kopell, 1990) have analyzed larger populations with local coupling, and a number of authors have studied the effects of global coupling in large populations (Golomb et al., 1992; Hansel et al., 1993) where no spatial organization is given to the network so that notions of distance are completely ignored. In contrast, we explore the effects of spatially decaying coupling and finite axonal conduction velocity on the behavior of a continuum of coupled neural oscillators. The crucial factors in our analysis are the relative sizes of the conduction velocity and the space constant for the decay of synaptic coupling. A large space constant coupled with a low velocity results in a loss of synchrony.

2. Methods

First we describe the phase model approach for approximating each neuron's voltage oscillation during repetitive firing with a single phase variable. When two such oscillators are coupled, the behavior of the system depends critically on the single interaction function chosen to describe the coupling. Next, we introduce a network model that consists of a continuum of these oscillators and that includes mechanisms that capture the effects of spatially decaying coupling and the effects of transmission delays due to finite axonal conduction velocity. We also derive equations for determining the stability of solutions describing the behavior of the network and analyze the behavior for two different interaction functions. The first is a sine interaction function sometimes used in coupled oscillator models of neural systems (Cohen et al., 1992). The second interaction function is derived from a compartmental model of a pyramidal cell developed using experimental data from a brain-slice preparation of rat piriform cortex.

2.1. Phase Model

Consider any cortical oscillator where the dynamics of the cell can be represented by

$$C\frac{dV(t)}{dt} = -I_{\text{Ion}}(V, \vec{w}) + I_{\text{Stim}} - I_{\text{Syn}}, \qquad (1)$$

where $V(t)$ denotes the membrane potential for the cell at time t, C is membrane capacity, I_{Ion} is the sum of voltage and time-dependent currents through the various ionic channel types, and $\vec{w}$ is the vector of auxiliary membrane variables such as intracellular calcium and the gating variables. We can assume that the stimulus I_{Stim} is constant and spatially homogeneous so that the neuron is capable of spontaneously oscillating in the absence of synaptic current (Rinzel and Ermentrout, 1992). Alternatively, one can hypothesize that the cell acts as an oscillator due to the local network interactions with inhibitory neurons as described in various models of cortical networks (Eeckman and Freeman, 1990; Whittington et al., 1995; Wilson and Bower, 1991, 1992). In either case, $V(t)$ denotes the oscillation of a single uncoupled oscillator, so that $V(t) \approx V(\theta(t))$ where $\theta(t)$ represents the periodic phase of the oscillator. If the intrinsic frequency of the

oscillator is ω, then the phase satisfies

$$\frac{d\theta(t)}{dt} = \omega. \tag{2}$$

This single-variable phase model approximates the repetitive behavior of the voltage oscillation, but no amplitude information is retained.

A synaptic current with no delay or spatial dependence has the form

$$I_{\text{Syn}}(t) = \bar{g}_{\text{Syn}} S[\hat{V}(t)](V(t) - V_{\text{Syn}}), \tag{3}$$

where $\bar{g}_{\text{Syn}}$ denotes the maximal conductance for the synapse, V_{Syn} is the synaptic reversal potential, and $S[\cdot]$ is some functional of the presynaptic voltage potential $\hat{V}(t)$ that provides the synaptic time course such as an alpha function. Now consider two oscillating cells identical to those of Eq. (1) that are coupled with no delay or spatial dependence:

$$\begin{aligned} C\frac{dV_1(t)}{dt} &= -I_{\text{Ion}}(V_1, \vec{w}_1) + I_{\text{Stim}} \\ &\quad - \bar{g}_{\text{Syn}} S[V_2(t)](V_1(t) - V_{\text{Syn}}) \end{aligned} \tag{4}$$

$$\begin{aligned} C\frac{dV_2(t)}{dt} &= -I_{\text{Ion}}(V_2, \vec{w}_2) + I_{\text{Stim}} \\ &\quad - \bar{g}_{\text{Syn}} S[V_1(t)](V_2(t) - V_{\text{Syn}}). \end{aligned} \tag{5}$$

If $\bar{g}_{\text{Syn}}$ is small, then it is possible to formally average the equations leading to a phase model for the interactions between the neurons (Ermentrout and Kopell, 1984; Kuramoto, 1984). This phase-reduction approach has been used by numerous authors in order to understand the dynamics of interacting neural oscillators in situations where the coupling is weak (Ermentrout and Kopell, 1991; Cohen et al., 1992). The phases of the oscillators in this coupled system satisfy

$$\frac{d\theta_1(t)}{dt} = \omega + \bar{g} H(\theta_2(t) - \theta_1(t)) \tag{6}$$

$$\frac{d\theta_2(t)}{dt} = \omega + \bar{g} H(\theta_1(t) - \theta_2(t)), \tag{7}$$

where $\bar{g}$ denotes the coupling strength and the interaction function $H(\cdot)$ is periodic and depends on the nature of the synaptic coupling and the uncoupled oscillation (Ermentrout and Kopell, 1990).

It is possible to numerically compute an interaction function that is representative of a particular connection by averaging the synaptic influence over the cycle of a model cell's oscillation. As the cell oscillates, any small perturbation will result in a phase shift that depends on the nature of the perturbation and the time in the cycle at which it occurred. We can compute a function called the phase response function by determining the phase shifts that result from infinitesimally small perturbations (Kuramoto, 1984; Hansel et al., 1995). We choose another function that describes the synaptic coupling or the form of the interaction. Then the interaction function is computed by averaging these two functions so that the net effect is a convolution of the phase response curve for the local response of an oscillator with the function that describes the coupling (Ermentrout, 1996). The resulting function can be decomposed into the first few Fourier components to provide an expression for $H(\cdot)$. An example is given below in Section 3.2.

Let $\phi(t) = \theta_2(t) - \theta_1(t)$, and consider the case where $H(\phi) = \sin(\phi)$. From Eqs. (6) and (7) we have

$$\frac{d\phi(t)}{dt} = \bar{g}(H(-\phi) - H(\phi)) = -2\bar{g}\sin(\phi). \tag{8}$$

Any solution $\bar{\phi}(t)$ to the equation $\dot{\phi}(t) = 0$ is a phase-locked solution to the system. In this case, the phase-locked solutions are the synchronous solution where $\phi(t) = 0$ and the solution corresponding to completely antiphasic behavior where $\phi(t) = \pi$. Linearizing near these fixed solutions, we obtain

$$\frac{d\phi(t)}{dt} \approx [-2\bar{g}H'(\bar{\phi})]\phi(t) = [-2\bar{g}\cos(\bar{\phi})]\phi(t). \tag{9}$$

Since $-2\bar{g}\cos(0) < 0$, the synchronous solution is stable. Similarly, the antiphase solution is unstable, since $-2\bar{g}\cos(\pi) > 0$. Thus, the sine interaction function is synchronizing when it governs the coupling of two identical oscillators. In contrast, the interaction function $H(\phi) = -\sin(\phi)$ is desynchronizing.

2.2. A Continuum Model

Now consider a continuous network of identical cells in one spatial dimension where the dynamics of each cell can be represented by Eq. (1). Let $V(x, t)$ denote the membrane potential for the cell at position x. Since there is a continuum of oscillators, the synaptic current of this cell depends on the synaptic influence of all other cells in the network. A spatial weight function $w(x)$ allows us to quantify the connectivity so that larger

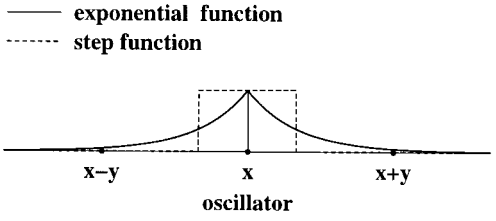

Figure 1. Schematic of the model connectivity for the oscillator at position x showing two possible weight functions.

values indicate areas with more synaptic influence on the oscillator at position x. Figure 1 shows a schematic of the network configuration with two possible weight functions. The representation for the synaptic current provided in Eq. (3) becomes

$$I_{\mathrm{Syn}}(x,t) = (V(x,t) - V_{\mathrm{Syn}})\frac{1}{\sigma}\int_{\Omega} w(|x-\hat{x}|/\sigma) \times \bar{g}_{\mathrm{Syn}}\, S[V(\hat{x},t)]\, d\hat{x}, \quad (10)$$

where $\hat{x}$ denotes a presynaptic oscillator, and we normalize $w(x)$ to integrate to one over the domain Ω. The space constant σ provides an additional coupling parameter. When it is small, coupling is local and strong; for large values of σ it is diffuse but long range.

We also want the synaptic current to depend on the axonal delay between the presynaptic and postsynaptic cells. Thus, Eq. (10) becomes

$$I_{\mathrm{Syn}}(x,t) = (V(x,t) - V_{\mathrm{Syn}})\frac{1}{\sigma}\int_{\Omega} w(|x-\hat{x}|/\sigma) \times \bar{g}_{\mathrm{Syn}} S[V(\hat{x}, t-|x-\hat{x}|/v)]\, d\hat{x}, \quad (11)$$

where v is the positive axonal velocity value, and the timing of $S[\cdot]$ depends on the distance between the presynaptic cell $\hat{x}$ and the postsynaptic cell x. The phase–reduction approach introduced in Section 2.1 has the advantage that delays in the temporal responses become phase shifts in the interaction function. Thus, the phase model for the continuous network is

$$\frac{\partial\theta(x,t)}{\partial t} = \omega + \frac{\bar{g}}{\sigma}\int_{-\infty}^{\infty} w(|y|/\sigma) H(\theta(x-y,t) - \theta(x,t) - |y|/v)dy, \quad (12)$$

where we have performed a change of variable letting $y = x - \hat{x}$ so that $|y|$ now represents the dimensionless distance between the oscillators, and the domain is the real line. We choose the real line so that Eq. (12) is solvable and the boundary effects are not relevant. Note that because w decays, the oscillators that are far away do not exert much influence. If we scale out the space constant, we obtain

$$\frac{\partial\theta(x,t)}{\partial t} = \omega + \bar{g}\int_{-\infty}^{\infty} w(|y|) H(\theta(x-y,t) - \theta(x,t) - |y|/\nu)dy, \quad (13)$$

where $\nu = v/\sigma$. When ν is large, the velocity is fast relative to the space constant of the association fibers. The parameter $1/\nu$ has dimensions of time. Thus, one can think of $|y|/\nu$ as an effective delay for the coupling between two oscillators that are the dimensionless distance $|y|$ from one another.

2.3. *Solutions and Stability*

Equation (13) has a one parameter family of traveling wave phase-locked solutions of the form

$$\theta(x,t) = \alpha x + \Omega_\alpha t \quad (14)$$

with frequency

$$\Omega_\alpha = \omega + \bar{g}\int_{-\infty}^{\infty} w(|y|) H(-\alpha y - |y|/\nu)dy, \quad (15)$$

where α is the nonnegative wave number. Thus, Ω_α represents the dispersion relation of frequency versus wavenumber. When $\alpha = 0$, we obtain the spatially homogeneous synchronous solution

$$\theta(x,t) = \Omega_0 t, \quad (16)$$

where

$$\Omega_0 = \omega + \bar{g}\int_{-\infty}^{\infty} w(|y|) H(-|y|/\nu)dy \quad (17)$$

and the phases are independent of x.

The particular values of ω and $\bar{g}$ do not affect the stability of the solution, so without loss of generality, let $\omega = 0$ and $\bar{g} = 1$. Let $p(x,t)$ denote a perturbation to a given solution. The behavior of the perturbation is governed by the linear variational equation

$$\frac{\partial p(x,t)}{\partial t} = \int_{-\infty}^{\infty} w(|y|) H'(-\alpha y - |y|/\nu) \times (p(x-y,t) - p(x,t))dy, \quad (18)$$

which has solutions of the form $p(x,t) = e^{\lambda_k t}e^{ikx}$. Thus, formal stability is assured if the real part of λ_k is negative for all k so that the perturbation decays. Substituting this expression for a solution into Eq. (18) and taking the real part, we find that

$$Re(\lambda_k) = \int_{-\infty}^{\infty} w(|y|)H'(-\alpha y - |y|/\nu) \times(\cos(ky) - 1)dy. \quad (19)$$

Since $\cos(0) - 1 = 0$, $Re(\lambda_0) = 0$ regardless of the parameter values of α and ν. This zero eigenvalue corresponds to the arbitrary phase shift of the synchronous solution. Thus, we only need $Re(\lambda_k) < 0$ for all $k \neq 0$ to assure stability.

2.4. *Compartmental Model*

Experimental data were obtained from a brain-slice preparation of rat piriform cortex using standard sharp-electrode intracellular recording procedures (Hasselmo and Bower, 1992). Current-clamp recordings from superficial pyramidal cells in layer II were taken at a variety of current levels ranging from levels at which no spiking occurred to levels high enough to cause rapid initial spiking followed by slower repetitive firing representing pronounced adaptation. A representative cell was chosen for further analysis.

The data obtained from the representative cell were used to construct a five-compartment model of a superficial pyramidal cell from the piriform cortex using the neural simulation program GENESIS version 2.0 (Bower and Beeman, 1995). Figure 2 depicts the structure of the model with compartments representing the distal dendrite in layer Ia, distal dendrite in layer Ib, proximal dendrite in layer Ib, soma, and basal dendrite. The active conductances were restricted to the soma compartment and include a fast-activating voltage-dependent sodium current (I_{Na}) and a delayed rectifier potassium current (I_{K-DR}) mediating the generation of simulated action potentials. They also include a noninactivating voltage-dependent potassium current (I_{K-M}), a calcium-dependent potassium current (I_{K-AHP}), and a high-threshold voltage activated calcium current (I_{Ca}) similar to those in other pyramidal cell models (Barkai and Hasselmo, 1994; Traub et al., 1991; Pinsky and Rinzel, 1994). The standard voltage-independent leak currents (I_{L-S} and I_{L-D}) are included where the current in the soma partially reflects impalement damage. The kinetics of the model conductances were initialized with parameters taken from a model of a hippocampal CA3 neuron (Traub et al., 1991). Then the parameters representing the maximal conductances of the ion channels as well as the kinetic parameters of the channels were systematically adjusted using an automated parameter-search method based on the genetic-algorithm technique (Vanier and Bower, 1995). The model reproduces the experimental spiking behavior very accurately for a wide range of currents as shown in Fig. 3. Panel C compares the firing frequency of the model data and experimental data following adaptation.

3. Results

In the section above, we define a model of a continuum of coupled oscillators where the chosen weight function determines the connectivity of the system and the chosen interaction function determines the type of coupling. Equation (14) provides a family of possible solutions that describe the behavior of the model and

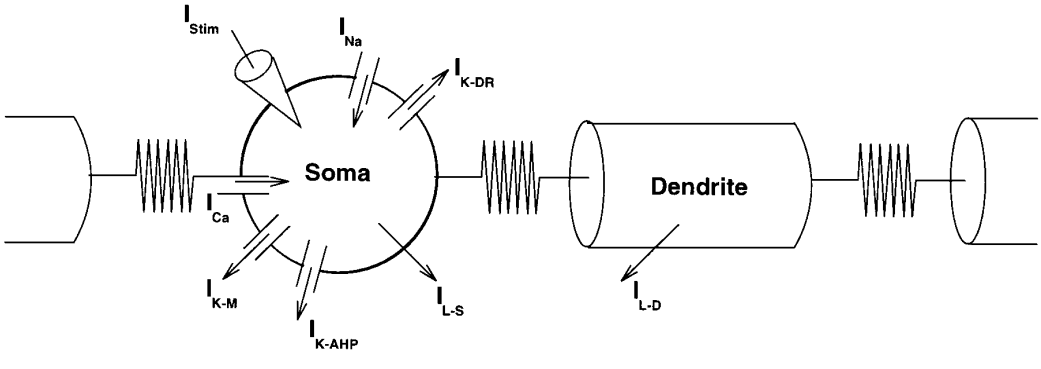

Figure 2. Schematic of the five-compartment model of a pyramidal cell from layer II of rat piriform cortex.

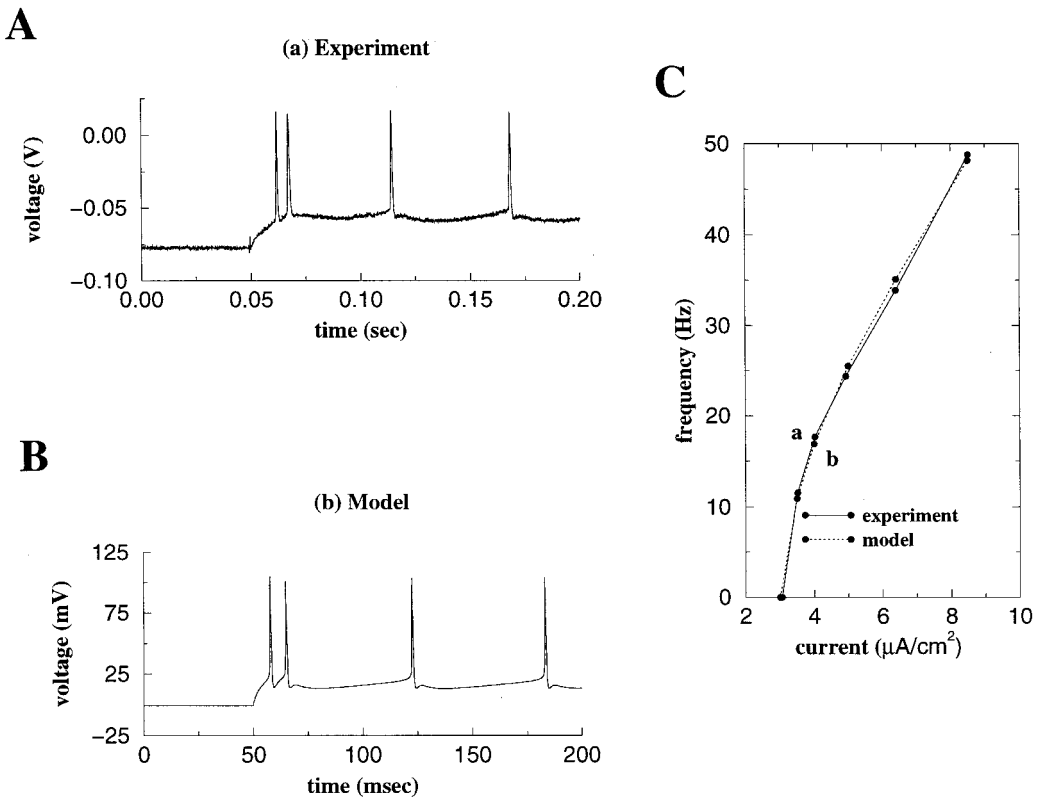

Figure 3. Voltage traces shown on the left in Panels **A** and **B** correspond to the points labeled *a* and *b* in Panel **C** which depicts the current-frequency relationships for the pyramidal cell model and the actual current injection data after adaptation. Panel **A** depicts the experimental response to a depolarizing current injection of 0.9984 nA to the soma beginning at time 0.05 sec. In Panel **B**, the model parameters mimic this applied current. I_{Stim} jumps from zero to 4.023 μA/cm^2 at time 50 msec.

depend on the parameters α and ν. For a given choice of parameters, Eq. (19) provides a means for determining the stability of the corresponding solution. Next we examine the effects of axonal delay in several specific situations by determining which solutions are stable for different function choices.

In general, we can express $H(\phi)$ as a Fourier series

$$H(\phi) = \sum_n a_n \cos(n\phi) + b_n \sin(n\phi), \qquad (20)$$

where the period of oscillation has been scaled so that $\phi \in [0, 2\pi]$. When the phase-reduction technique is used for oscillations that emerge through a normal Hopf bifurcation, the phase interaction has only one Fourier mode. So, for some neural oscillators, the interaction function $H(\phi) = p\sin(\phi) + q\cos(\phi)$ discussed in Section 3.1 below provides a good approximation. However, some reductions require several Fourier modes which can lead to dynamical phenomena that are not observed with a single-mode approximation (Hansel et al., 1993). In Section 3.2, we use the biophysical model of the pyramidal cell described in Section 2.4 to derive a more realistic interaction function with higher modes. We then perform the stability calculations for the continuum model with this interaction function.

Since we are interested in cortical dynamics, we consider our coupled oscillator model to serve as an approximation for a biological system where the cells act as oscillators due to the local network interactions with inhibitory neurons as described in various models of cortical networks (Eeckmann and Freeman, 1990; Whittington et al., 1995; Wilson and Bower, 1991, 1992). We now make the simplifying assumption that these oscillators influence one another through excitatory synaptic connections. For both of the interaction functions that we will examine, we consider the two types of weight function shown in Fig. 1. The step function simulates the effects of purely local

connectivity. In contrast, the exponential weight function captures the effects of spatially decaying coupling with some long-range connectivity.

3.1. *Sine Interaction Function*

We return to the case of a purely odd sine interaction function $H(\phi) = \sin(\phi)$ and consider the effects of delay in the continuum model with the exponential weight function $w(y) = \exp(-y)/2$. To determine the stability of the synchronous solution, we let $\alpha = 0$ and substitute these values into Eq. (19). Examining this stability equation, we find that as ν decreases it reaches a critical value $\nu = \sqrt{3}$. Below this value a band of unstable modes occurs near $k = 0$ where $Re(\lambda_k) > 0$ and the synchronous solution is unstable. Calculating $Re(\lambda_k)$ to determine the stability of a traveling wave solution where $\alpha \neq 0$ is more tedious, but the results are similar. The graphs of the stability equations for two solutions where $\nu = 1$ are shown in Panel A of Fig. 4. For this parameter value, the synchronous solution with $\alpha = 0$ is unstable since $Re(\lambda_k) > 0$ near $k = 0$ as shown by the solid curve. In contrast, the traveling wave solution with wavenumber $\alpha = 1$ is stable as shown by the dashed curve. For each choice of ν, there is some range of α values for which the solution is stable. In Panel B, the region between the two curves is the region of stable solutions for a range of positive ν values. For smaller values of ν corresponding to larger delays, the synchronous solution loses stability.

Now consider an interaction function with an even component, $H(\phi) = p\sin(\phi) + q\cos(\phi)$. Once again let $w(y) = \exp(-y)/2$ and $\alpha = 0$, and we use Eq. (19) to examine the stability of the synchronous solution. If we choose a value of ν for which the synchronous solution is stable when $q = 0$, then the stability holds for values of q in some neighborhood of zero. Thus, for $q \in [-1, 1]$, we find that the region of stability is qualitatively similar to the region described above for the pure sine function.

Next consider the case of the step weight function corresponding to purely local excitatory coupling. When $H(\phi) = \sin(\phi)$ we obtain the region of stable solutions shown in Fig. 5. Note that synchrony remains stable for much smaller ν values corresponding to large delays. Unlike the case of the exponential weight function, in the region where the wave solutions are stable, the synchronous solution is also stable. Thus, in the case of purely local coupling, the behavior of the system is heavily dependent on the initial conditions.

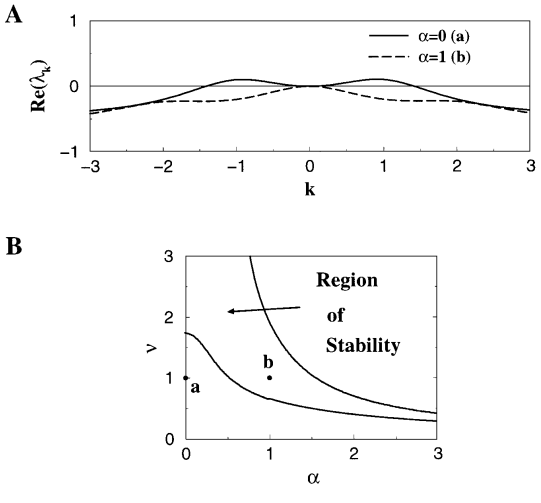

Figure 4. **A**: $Re(\lambda_k)$ for the synchronous solution where $\alpha = 0$ and the traveling wave solution with wavenumber $\alpha = 1$ for $\nu = 1$. In this case we use the sine interaction function and the exponential weight function. Note that the synchronous solution is unstable since $Re(\lambda_k) > 0$ near $k = 0$. In contrast, the traveling wave solution with wavenumber $\alpha = 1$ is stable. **B**: Region of stable solutions for a range of positive parameter values ν. The point labeled *a* corresponds to the solid curve in Panel A, and the point labeled *b* corresponds to the dashed curve.

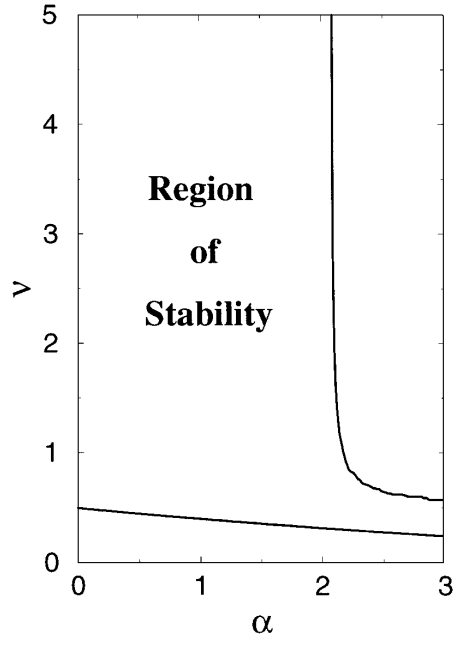

Figure 5. Region of stable solutions for a range of positive parameter values ν for the sine interaction function with a step weight function.

3.2. Pyramidal Cell Interaction Function

Now we derive a more realistic interaction function based on the compartmental model described in Section 2.4. The pyramidal cell model has a current balance equation for each of the five compartments and additional equations representing the dynamics of the gating variables for the various ionic currents in the soma. The ionic currents are

$$\begin{aligned} I_{Na}(V,m,h) &= \bar{g}_{Na} m^2 h (V - V_{Na}) \\ I_{K-DR}(V,n) &= \bar{g}_{K-DR} n (V - V_K) \\ I_{Ca}(V,s,r) &= \bar{g}_{Ca} s^2 r (V - V_{Ca}) \\ I_{K-AHP}(V,q) &= \bar{g}_{K-AHP} q (V - V_K) \\ I_{K-M}(V,w) &= \bar{g}_{K-M} w (V - V_K) \\ I_{L-S}(V) &= \bar{g}_{L-S} (V - V_L) \\ I_{L-D}(V) &= \bar{g}_{L-D} (V - V_L), \end{aligned} \tag{21}$$

where each of the kinetic equations for the gating variables m, h, n, s, r, q, and w takes the form

$$\frac{dy}{dt} = \frac{y_\infty(u) - y}{\tau_y(u)}. \tag{22}$$

Values for $y_\infty(u)$ and $\tau_y(u)$ for each gating variable are provided in the Appendix. In most cases $u = V$; the exception is the case of the calcium-dependent potassium current where $y = q$ and $u = Ca$. The variable Ca represents the intracellular free calcium level, and the equation for Ca handling in the soma compartment is

$$\frac{dCa}{dt} = -BI_{Ca} - Ca/\tau_{Ca}, \tag{23}$$

where B determines the rate of increase of intracellular calcium due to the inward calcium channel current and the second term represents the depletion of Ca as an exponential decay with time constant τ_{Ca}.

For the purposes of the coupled oscillator model, we are interested in regular repetitive firing, so we consider the behavior of the pyramidal cell model after adaptation has occurred. We use the model to derive an interaction function using the technique described in Section 2.1 where the numerical computations were performed using the software XPPAUT. The synaptic influence of a connection in the compartment representing the proximal dendrite in layer Ia is averaged over the cycle of a cell's oscillation by numerically computing a convolution of two functions. The first function is the adjoint or the phase response curve for the local response of the oscillator to perturbations, and the second is a synaptic coupling function similar to the synaptic current described in Eq. (3). The computed interaction function depends on the frequency of the oscillation; thus, it depends on the amount of applied current. The inset in Fig. 6 shows the voltage trace for a single oscillation when $I_{\text{Stim}} = 7\ \mu\text{A/cm}^2$ in the model. Note that for this current injection value, the period of the oscillation is $T = 25.8$ ms resulting in a frequency of approximately 40 Hz. The solid curve in the larger graph shows the derived interaction function for a synaptic current where $\bar{g}_{\text{Syn}} = 1\ \text{mS/cm}^2$, $V_{\text{Syn}} = 30$ mV, and the synaptic time course is equivalent to the dual exponential function

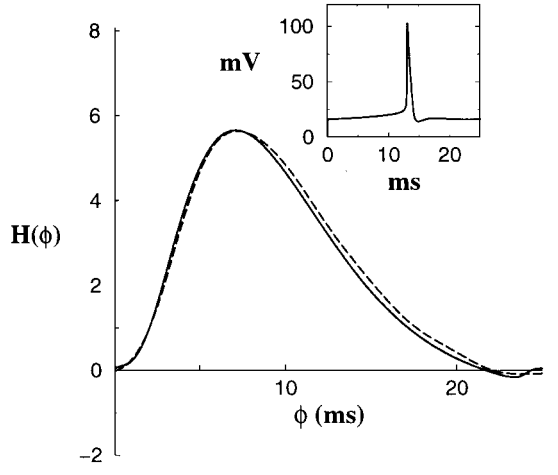

Figure 6. Voltage trace (inset) and interaction function $H(\phi)$ for two synaptically coupled pyramidal cell neurons where ϕ represents the phase difference between the presynaptic and postsynaptic neurons. The dashed curve shows the approximation to the interaction function used in the calculation in Section 3.2

$$f(t) = 2.75 \frac{\exp(-t/\tau_1) - \exp(-t/\tau_2)}{\tau_1 - \tau_2}, \tag{24}$$

where $\tau_1 = 2.8$ and $\tau_2 = 0.65$.

The interaction function can be decomposed into the first few Fourier components to provide the expression

$$H(\phi) = \sum_{n=0}^{5} a_n \cos(2\pi n\phi/T) + b_n \sin(2\pi n\phi/T) \tag{25}$$

for $\phi \in [0, T]$ where $a_0 = 2.28314$, $a_1 = -1.5457$, $a_2 = -0.738241$, $a_3 = -0.0929315$, $a_4 = 0.0345372$, $a_5 = 0.0440749$, $b_0 = 0$, $b_1 = 2.28948$, $b_2 =$

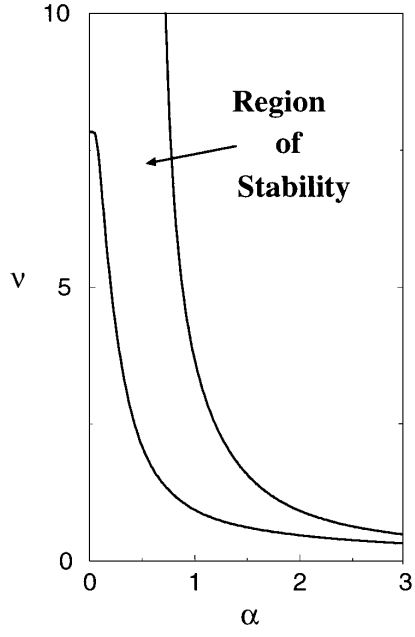

Figure 7. Region of stability for the continuum model using the pyramidal cell interaction function and exponential weight function.

-0.248993, $b_3 = -0.228386$, $b_4 = -0.0961023$, and $b_5 = -0.0353857$. This approximation to the interaction function appears as a dashed curve in Fig. 6. In Section 3.1, we determined the region of stability for a sine interaction function using an exponential weight function. We apply the same technique to the interaction function shown above and obtain similar results which are shown in Fig. 7. As before, a sufficient decrease in the value of ν results in increased delay and a loss of stability for the synchronous solution.

When we calculate the region of stability for the interaction function derived from the pyramidal cell with the step weight function, we obtain results very similar to those shown in Fig. 5 for the sine interaction function. The similarity between the results for the two functions suggests that the exact nature of the individual excitatory interactions is unimportant. The type of connectivity and the presence of delay have much more influence on the global behavior of the system.

The stability results described above are for an infinite domain. We calculate that for both interaction functions examined above, the same qualitative results hold for a finite domain system. We compute solutions using a simulation which discretizes the domain of the continuum model into 100 subintervals and uses initial conditions which are randomly distributed near a particular solution. As predicted by the stability analysis, the oscillators lose synchrony among their phases for small ν values corresponding to larger delays when long-range connections are included. We see the same qualitative behavior for other types of boundary conditions; however, the value of ν corresponding to the change in stability varies with the number of subintervals and the choice of boundary conditions. One should also note that one of the effects of multiple coupling is to make a system of coupled oscillators more stable to perturbations in the local natural frequencies (Kopell et al., 1990). Although we make the assumption that the oscillators in the continuum model are identical with frequency ω, we would expect the stability results to hold for nonidentical oscillators with frequencies distributed about ω. This was verified with simulations.

4. Discussion

The mechanism we describe in this article suggests that local excitatory connections are synchronizing, but distant ones produce phase shifts between cells due to the finite axonal conduction time. In our model, the parameter $1/\nu = \sigma/v$ characterizes the effective delay. When $1/\nu$ is small corresponding to strong local connectivity or fast fibers in the network, synchrony is stable. However, as this delay grows larger, the synchronous solution loses stability and the result is the appearance of traveling phase waves. The similarities between the stable regions for the two types of interaction function suggest that these results are robust and demonstrate the importance of considering the effects of delay in cortical models. In addition, our approach provides a novel means of implementing distance-dependent delays that is particularly useful due to the current prevalence of coupled oscillator models.

The simplifications and assumptions necessary for creating a coupled oscillator model cause our results to be qualitative rather than quantitative in nature. However, they are consistent with the oscillatory behavior observed in many neurobiological systems. One example is the olfactory cortex, which tends to exhibit traveling waves of oscillations (Haberly, 1985; Freeman, 1978). Long-range synaptic interactions are prevalent among pyramidal cells in the olfactory cortex (Gray, 1994), and slow velocities generate a distribution of time delays as long as 20 ms across the olfactory cortex in rat (Haberly, 1985). Our results suggest that the slower axonal velocities and long-range excitatory connections are capable of supporting the observed

traveling waves of oscillatory activity initiated by the directional lateral olfactory tract inputs. Wilson and Bower describe models of the piriform cortex (1992) and the primary visual cortex (1991) that include axonal delays. We can examine the results of these simulations in an analytical framework and explore the manner in which axonal delay determines the network behavior. In both versions of their cortical models, oscillations arise from afferent input tuned by a feedback inhibitory loop. The long-range connections in the piriform cortex simulations result in phase lags consistent with axonal delays. In their visual cortex model the connectivity is more local. This model exhibits synchrony as a result of synchronous stimulation among sites along a bar. When they reduced the axonal conduction velocity, the oscillations remained synchronous. These results are consistent with our model where the behavior is dependent on the initial conditions for the case of purely local coupling.

In the visual cortex, neurons exhibit synchronous activity between cells with a spatial separation of up to 7 mm in cat as well as between the two different cerebral hemispheres (Engel et al., 1991). The interhemispheric synchronization is stimulus dependent, variable in frequency, and absent in animals with a severed corpus callosum. Attempting to model this phenomenon, Ritz et al. (1994) are able to demonstrate synchrony in a network simulation with all-to-all coupling provided that the average interhemispheric delay does not exceed 5 ms. The simulation studies of König and Schillen (1991) estabilish a 0 phase lag using reciprocal coupling. However, their model requires that the local circuit time-constant match the delay time between neighboring circuits and accomplishes this with unrealistically long delays between the onset of pyramidal cell firing and the excitation of nearby interneurons. Traub et al. (1996) demonstrate synchrony in a more biologically feasible model consisting of a chain of interconnected cell groups where the local circuit delay occurs due to the doublet firing of interneurons. In their model the conduction delay can total 20 ms from one end of the chain to the other; however, the intergroup delays do not exceed 5 ms. Bush and Sejnowski (1996) obtain a similar result with a realistic network model of cortical columns where synaptic delays exceeding 5 ms abolish synchrony between columns. It remains to be determined whether any one of these models provides a sufficient means of generating interhemispheric synchronization. Our analytical model shows that regardless of the mechanism producing individual oscillations, synchrony can no longer be stable once the delays become too large when long-range connections are present.

Our results are also consistent with the oscillatory behavior observed in other biological systems where axons can provide functionally significant delays in conduction. In systems that perform temporal coding where synchronous phase-locking is important, morphology is well suited to this function including thick axons with fast propagation velocities. Examples are the time-coding electrosensory system of the electric fish and the auditory system of the barn owl and echolocating bats (Carr, 1993). It is also interesting to note that biological systems exhibit evidence of compensatory mechanisms that overcome the phase shifts or synchrony inherent to axon length and conduction velocity. Compensatory axonal delay line mechanisms include equalization of path length, differences in conduction velocity, and localized delays determined by branch variations (Waxman, 1975). When delay is needed in local circuits where it would be inefficient to create them by varying axonal path length, local inhibitory circuits are involved in the manner described above to overcome the tendency of local connections to synchronize (Carr, 1993). Examples include the detection of echo delays in the bat auditory cortex (Olsen and Suga, 1991) and the X-lagged cell response in the visual thalamus (Mastronade, 1987).

Additional studies show that delays in coupling result in a loss of stability for synchronized oscillators. The delays in these models occur due to the persistence of the postsynaptic potential, which causes the effect of the presynaptic oscillator to be felt long after it has fired. Wang and Rinzel (1993) show that for large clusters of thalamic neurons with inhibitory coupling, synaptic persistence can lead to synchronization. Similarly van Vreeswijk et al. (1994) show that in a pair of mutually coupled oscillators, this effective delay results in the destabilization of synchrony for excitatory coupling and the stabilization of synchrony for inhibitory coupling. Recently, Ermentrout and Kopell (1994) showed that a chain of oscillators with local excitatory coupling and long-range inhibitory coupling can produce traveling waves if the long-range connections are sufficiently strong to cause a destabilization of synchrony. The mechanism we describe in this article is functionally similar, although the delays are a consequence of the finite conduction time of the axons.

Appendix

The functions that determine the kinetic equations for the gating variables are listed below. In some cases we give the functions in the form $\alpha_y(u)$ and $\beta_y(u)$ where $y_\infty(u) = \alpha_y(u)/(\alpha_y(u) + \beta_y(u))$ and $\tau_y(u) = 1/(\alpha_y(u) + \beta_y(u))$.

$$\alpha_m(V) = \frac{0.32(30.1 - V)}{\exp(0.25(30.1 - V)) - 1}$$

$$\beta_m(V) = \frac{0.28(V - 57.1)}{\exp((V - 57.1)/5.0) - 1}$$

$$\alpha_h(V) = 0.128\exp((34 - V)/18)$$

$$\beta_h(V) = \frac{4}{\exp((57 - V)/5) + 1}$$

$$\alpha_n(V) = \frac{0.059(52.1 - V)}{\exp((52.1 - V)/5) - 1}$$

$$\beta_n(V) = 0.925\exp(0.925 - 0.025V)$$

$$\alpha_s(V) = \frac{0.912}{\exp(-0.072(V - 82)) + 1}$$

$$\beta_s(V) = \frac{0.0114(V - 68.1)}{\exp((V - 68.1)/5) - 1}$$

$$\alpha_r(V) = 1.1\min(0.005, 0.005\exp(-(V - 17)/20))$$

$$\beta_r(V) = 1.1(0.005 - \alpha_r(V))$$

$$q_\infty(Ca) = (0.0005Ca)^2$$

$$\tau_q(Ca) = \frac{0.0338}{\min(.00001Ca, .01) + .001}$$

$$w_\infty(V) = \frac{1}{\exp(-(V - 42)/10) + 1}$$

$$\tau_w(V) = \frac{303.03}{3.3\exp((V - 42)/20) + \exp(-(V - 42)/20)}$$

The standard values of the parameters for the pyramidal cell model are given below. The maximal conductances in units of mS/cm^2 are $\bar{g}_{Na} = 221$, $\bar{g}_{K-DR} = 47$, $\bar{g}_{Ca} = 8.5$, $\bar{g}_{K-AHP} = 7$, and $\bar{g}_{K-M} = 6.5$. In the soma $\bar{g}_{L-S} = 2$, and $\bar{g}_{L-D} = 0.05$ in the dendrite compartments. The reversal potentials in units of mV are $V_{Na} = 132$, $V_K = -13$, $V_L = 0$, and $V_{Ca} = 197$. The capacitance is $C_M = 0.8\ \mu$F/cm^2. The calcium handling parameters are $B = 3$ and $\tau_{Ca} = 60$ ms.

Acknowledgments

We thank J. Rinzel, D. Golomb, and C. Carr for fruitful discussions and helpful comments. G.B. Ermentrout is supported in part by NIMH RO1-MH47150 and also by NSF DMS-96-728. S.M. Crook, M.C. Vanier, and J.M. Bower are supported in part by NSF BIR 94-00878. XPPAUT files that simulate the single-cell model described in this article are available on request.

References

Barkai E, Hasselmo ME (1994) Modulation of the input/output function of rat piriform cortex pyramidal cells. *Journal of Neurophysiology* 72:644–658.

Bower JM (1995) Reverse engineering the nervous system: an in vivo, in vitro, and in computo approach to understanding the mammalian olfactory system. In: S Zornetzer, J Davis, C Lau, eds., An Introduction to Neural and Electronic Networks, Academic Press, New York, pp. 3–28.

Bower JM, Beeman D (1995) The Book of GENESIS: Exploring Neural Models with the GEneral NEural Simulation System. Telos/Springer, Santa Clara, CA.

Carr CE (1993) Processing of temporal information in the brain. *Annual Reviews in Neuroscience* 16:223–243.

Cohen A, Ermentrout GB, Kiemel T, Kopell N, Sigvardt KA, Williams TL (1992) Modeling of intersegmental coordination in the lamprey central pattern generator for locomotion. *Trends in Neuroscience* 15:434–438.

Eeckman FH, Freeman WJ (1990) Correlations between unit firing and eeg in the rat olfactory system. *Brain Research* 528:238–244.

Engel AK, König P, Kreiter AD, Singer W (1991) Interhemispheric synchronization of oscillatory responses in cat visual cortex. *Science* 252:1177–1179.

Ermentrout GB (1996) Type I membranes, phase resetting curves, and synchrony. *Neural Computation* 8:979–1001.

Ermentrout GB, Kopell N (1984) Frequency plateaus in a chain of weakly coupled oscillators. *SIAM Journal on Mathematical Analysis* 15:215–237.

Ermentrout GB, Kopell N (1990) Oscillator death in systems of coupled neural oscillators. *SIAM Journal of Applied Mathematics* 50:125–146.

Ermentrout GB, Kopell N (1991) Multiple pulse interactions and averaging in systems of coupled neural oscillators. *Journal of Mathematical Biology* 29:195–217.

Ermentrout GB, Kopell N (1994) Inhibition produced patterning in chains of coupled nonlinear oscillators. *SIAM Journal on Applied Mathematics* 54:478–507.

Freeman WJ (1978) Spatial properties of an EEG event in the olfactory bulb and cortex. *Electroencephalography and Clinical Neurophysiology* 44:586–605.

Golomb D, Hansel D, Sompolinsky H (1992) Clustering in globally coupled phase oscillators. *Physical Review A* 45:3516–3530.

Gray CM (1994) Synchronous oscillations in neuronal systems: mechanisms and functions. *Journal of Computational Neuroscience* 1:11–38.

Gray CM, König P, Engel AK, Singer W (1989) Oscillatory responses in cat visual cortex exhibit inter-columnar synchroniztion which reflects global stimulus properties. *Nature* 338:334–337.

Haberly LB (1985) Neuronal circuitry in olfactory cortex: anatomy and functional implications. *Chem. Senses* 10:219–238.

Hansel D, Mato G, Meunier C (1993) Clustering and slow switching in globally coupled phase oscillators. *Physical Review E*, 48:3470–3477.

Hansel D, Mato G, Meunier C (1995) Synchrony in excitatory neural networks. *Neural Computation* 7:192–210.

Hasselmo ME, Bower JM (1992) Cholinergic suppression specific to intrinsic not afferent fiber synapses in rat piriform (olfactory) cortex. *Journal of Neurophysiology* 67:1222–1229.

König P, Schillen TB (1991) Stimulus-dependent assembly formation of oscillatory responses: I. Synchronization. *Neural Computation* 3:155–166 .

Kopell N, Ermentrout GB (1986) Symmetry and phaselocking in chains of weakly coupled oscillators. *Communications on Pure and Applied Mathematics* 39:623–660.

Kopell N, Zhang W, Ermentrout GB (1990) Multiple coupling in chains of oscillators. *SIAM Journal on Mathematical Analysis*, 21:935–953.

Kuramoto Y (1984) Chemical Oscillations, Waves, and Turbulence. Springer, New York.

Mastronade DN (1987) Two classes of single-input X-cells in cat lateral geniculate nucleus. i. receptive field properties and classification of cells. *Journal of Neurophysiology* 57:357–380.

Olsen JF, Suga N (1991) Combination-sensitive neurons in the medial geniculate body of the mustached bat: encoding of target range information. *Journal of Neurophysiology* 65:1275–1296.

Pinsky PF, Rinzel J (1994) Intrinsic and network rhythmogenesis in a reduced Traub model for CA3 neurons. *Journal of Computational Neuroscience* 1:39–60.

Rinzel J, Ermentrout GB (1992) Analysis of neural excitability. In Koch C, Segev I, eds. Methods in Neuronal Modeling, The MIT Press, Cambridge, MA, pp. 135–169.

Ritz R, Gerstner W, Fuentes U, van Hemmen JL (1994) A biologically motivated and analytically soluble model of collective oscillations in the cortex ii. application to binding and pattern segmentation. *Biological Cybernetics* 71:349–358.

Traub RD, Wittington MA, Stanford IM, Jefferys JGR (1996) A mechanism for generation of long-range synchronous fast oscillations in the cortex. *Nature* 383:621–624.

Traub R, Wong R, Miles R, Michelson H (1991) A model of a CA3 hippocampal pyramidal neuron incorporating voltage-clamp data on intrinsic conductances. *Journal of Neurophysiology* 66:635–649.

Vanier MC, Bower JM (1995) A comparison of automated parameter-searching methods for neural models. In JM Bower. Computational Neuroscience, Academic Press, pp. 477–482.

van Vreeswijk C, Abbott LF, Ermentrout GB (1994) When inhibition not excitation synchronizes neural firing. *Journal of Computational Neuroscience* 1:313–322.

Wang XJ, Rinzel J (1993) Spindle rhythmicity in the reticularis thalami nucleus: Synchronization among mutually inhibitory neurons. *Neuroscience* 53:899–904.

Waxman SG (1975) Integrative properties and design principles of axons. *International Reviews in Neurobiology* 18:1–40.

Whittington MA, Traub RD, JGR Jefferys (1995) Synchronized oscillations in interneuron networks driven by metabotropic glutamate receptor activation. *Nature* 373:612–615.

Wilson M, Bower JM (1991) A computer simulation of oscillatory behavior in primary visual cortex. *Neural Computation* 3:498–509.

Wilson M, Bower JM (1992) Cortical oscillations and temporal interactions in a computer simulation of piriform cortex. *Journal of Neurophysiology* 67:981–995.